Recent Improvements to Release III of the K&C Concrete Model

Joseph M. Magallanes[1], Youcai Wu[1], L. Javier Malvar[2], and John E. Crawford[1]

[1]Karagozian & Case, Burbank, CA
[2]Naval Facilities Engineering Service Center, Port Hueneme, CA

Abstract

Recent improvements are made to Release III of the Karagozian & Case (K&C) concrete model. This three-invariant plasticity and damage-based constitutive model is widely used to model a number of materials, including normal and lightweight concrete, concrete masonry, and brick masonry, to compute the effects of quasi-static, blast, and impact loads on structures. This most recent version of the model, made available starting with LS-DYNA® v971 as *MAT_CONCRETE_DAMAGE_REL3, incorporates a number of improvements to the original model that are described in this paper. The model now exhibits: (a) an automatic input capability for generating the data for generic concrete materials and (b) methods to reduce mesh-dependencies due to strain-softening. A simple method is implemented to regularize the fracture energy by internally scaling the damage function for the generic concrete model parameters. For user-defined material parameters, a method is developed that can preserve fracture energy using the results of either single-element or multi-element simulations. Finally, concrete loading rate effects are discussed and guidance is provided on properly modeling such effects with the model.

1. Introduction

The K&C concrete (KCC) material model was first released in 1994 [1-3]. This first version represented a significant overhaul of the concrete material model (Model 16) in the DYNA3D finite element (FE) program. This overhaul included (1) adding a third, independent failure surface based on a Willam-Warnke three-invariant formulation (a change from the original two-invariant formulation), (2) introducing a radial stress path for the strain rate enhancement algorithm, (3) adding a fracture energy dependent strain in tension, and (4) fixing several major discrepancies in the original model.

The second release of the KCC model was released in 1996 [4]. The Release II model extended the previous model to include shear dilation (i.e., increase in volume due to shearing). The formulation introduced in this version allowed the model to be partially associative, fully associative, or non-associative, facilitating a more accurate representation of the behavior of reinforced concrete structures. In addition, the strain rate effect algorithm was modified to allow for implementation of different strain rate enhancement factors, or dynamic increase factors (DIFs), in tension and compression [5].

This third release of the model [6], made available in LS-DYNA starting with v971 as *MAT_CONCRETE_DAMAGE_REL3 [7-8], incorporates a number of improvements to the original formulation, which are described in this paper. First, the automatic input capability for generating the model parameters for "generic" concrete materials is discussed. Second, methods included in the model to reduce mesh-dependencies due to strain-softening are described. Finally, concrete loading rate effects are discussed and guidance is provided on properly modeling rate effects with the model.

The principal advantage that this model provides, in comparison with other constitutive models used for concrete-like materials, is that it is relatively simple and numerically robust. It is capable of reproducing key concrete behaviors critical to blast and impact analyses and is also quite easily calibrated to laboratory data. The modeling capabilities afforded by the improvements in Release III are evidenced in numerous recent studies in the literature [9-12]. The discussions presented in this paper are especially warranted in light of recent material testing conducted by K&C and others and to further detail features of the model.

2. Automatic Parameter Generation

Under sponsorship of various U.S. Department of Defense agencies, extensive mechanical characterization tests were completed for several concrete materials. Material tests included unconfined uniaxial compression and tension tests, triaxial compression tests under various levels of confinement, hydrostatic compression tests, and a number of strain path tests. These types of material characterization tests are described in [13].

Default values for the KCC model were derived based on these and other data derived from the literature (e.g., see [14]). The default concrete exhibited an average compressive strength, f_c', slightly over 45 MPa (or 6,500 psi).

To generalize the KCC model for other concrete materials, its parameters are adjusted using the concrete strength parameters to obtain the appropriate relationships between the concrete properties, e.g., relationships between tensile and compressive strength, and between bulk modulus and compressive strength, among others [15]. For the deviatoric strength, the KCC model uses a simple function to characterize three independent failure surfaces that define the yield, maximum, and residual strength of the material. Three parameters a_{0i}, a_{1i}, and a_{2i} (9 parameters total for the three surfaces) define each of the failure surfaces:

$$F_i(p) = a_{0i} + \frac{p}{a_{1i} + a_{2i} \cdot p} \tag{1}$$

where, p is the pressure (i.e., mean normal stress) and F_i is the ith of three failure surfaces.

For hardening, the plasticity surface used in the model is interpolated between the yield and maximum surfaces based on the value of the damage parameter, λ. For softening, a similar interpolation is performed between the maximum and residual surfaces.

The parameters in Eqn. (1) were calibrated to the original data and provide a best fit for that material; these are designated $a_{0i}\big|_o$, $a_{1i}\big|_o$, and $a_{2i}\big|_o$. The scaling coefficient, r, is defined as the ratio of the interpolated f_c' (i.e., the material strength one desires to model) to the compressive strength of the original material characterized in the laboratory, f_{co}', or:

$$r = \frac{f_c'}{f_{co}'} \tag{2}$$

For any selection of f_c', the failure surface parameters are scaled using r as follows:

$$a_{0i} = a_{0i}\big|_o \cdot r \tag{3a}$$

$$a_{1i} = a_{1i}\big|_o \tag{3b}$$

$$a_{2i} = a_{2i}\big|_o / r \tag{3c}$$

The failure surface obtained from the generic concrete is shown in Fig. 1a for three different concrete compressive strengths. The Equation of State (EOS) is also scaled using r and is shown in Fig. 1b for the same three concrete compressive strengths.

(a) Maximum failure surface. (b) Equation of state.
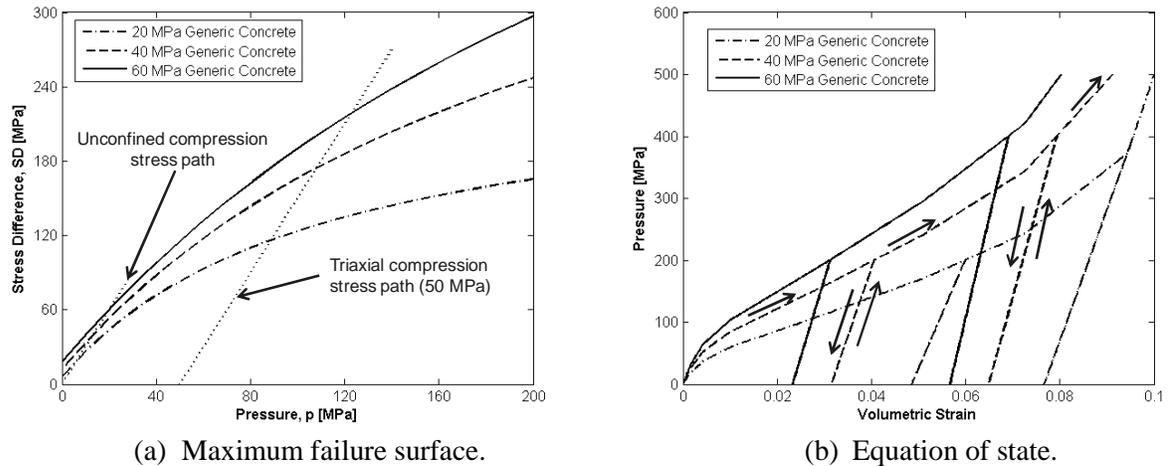
Fig. 1. Strength and volumetric responses obtained from the generic concrete model.

The tension softening parameter, b_2, is also scaled using simple relationships for concrete. The b_2 model parameter, which controls the behavior of the model in strain softening, is adjusted to obtain the fracture energies (G_f) recommended by the CEB [16]. These are shown in Table 1. In Release III, the fracture can be entered in one of two ways. First, a user may directly enter b_2 values, using Table 1 as guidance. Alternatively, the model can internally compute estimates for the fracture energies of Table 1 by entering f_c' and the maximum aggregate size (*MAS*).

This automatic parameter generation capability was developed to provide analysts with a simple tool from which to model concrete when little is known other than the concrete's compressive strength. There are, naturally, a number of limitations to this feature:

- Recent experimental studies have shown that concrete's shear strength can be quite variable, especially for confining pressures greater than 50 MPa [13, 17-19]. Based on these studies, a concrete's failure surface can be affected by a number of other factors including the porosity and moisture content. Unfortunately, there is currently insufficient data from which to formulate functions for these other parameter effects.

- The volumetric response (i.e., the EOS) for concrete is also variable. Although material characterization tests are expensive and time-consuming, calibrating the KCC model to specific material characterization data may be warranted in some situations.

- The superficial similarities between concrete and a number of concrete-like materials such as concrete and brick masonry tempt many to use the generic concrete fit to model masonry structures. Although the materials are indeed similar, the behaviors of concrete and brick masonry have subtle but important differences. The main difference is the lack of coarse aggregate in the latter—coarse aggregate tends to slow down crack propagation resulting, for example, in higher tensile strengths. Concrete masonry tends to behave more akin to

Table 1. Mode I tensile fracture energies for concrete based on CEB recommendations.

Grade			C12	C20	C30	C40	C50	C60	C70	C80
f_c' cylinder [MPa]			12	20	30	40	50	60	70	80
f_c' cylinder [Ksi]			1.740	2.901	4.351	5.802	7.252	8.702	10.153	11.603
f_c' cube [MPa]			15	25	37	50	60	70	80	90
f_c' cube [Ksi]			2.176	3.626	5.366	7.252	8.702	10.153	11.603	13.053
	Max. agg. size									
	[mm]	[in]								
	8	0.315	40.5	50.2	61.9	73.2	84.2	94.7	104.9	114.7
G_f	12.7	0.5	45.4	56.9	70.7	83.6	95.6	106.8	117.1	126.6
[N/m]	16	0.630	48.6	61.3	76.3	90.2	103.0	114.7	125.3	134.9
	19.05	0.75	51.4	64.9	81.0	95.7	109.2	121.5	132.6	142.5
	25.4	1	56.8	71.7	89.4	105.7	120.7	134.5	147.0	158.1
	32	1.260	61.7	77.4	96.1	113.7	130.4	146.0	160.6	174.2
	Max. agg. size									
	[mm]	[in]								
	8	0.315	0.232	0.287	0.353	0.418	0.481	0.541	0.599	0.655
G_f	12.7	0.5	0.259	0.325	0.404	0.477	0.546	0.610	0.669	0.723
[lbs/in]	16	0.630	0.277	0.350	0.436	0.515	0.588	0.655	0.716	0.770
	19.05	0.75	0.293	0.371	0.462	0.547	0.624	0.694	0.757	0.814
	25.4	1	0.324	0.409	0.510	0.603	0.689	0.768	0.839	0.903
	32	1.260	0.352	0.442	0.549	0.650	0.745	0.834	0.917	0.995
	Max. agg. size									
	[mm]	[in]								
	8	0.315	1.40	1.88	2.11	2.20	2.23	2.25	2.25	2.25
b_2	12.7	0.5	1.02	1.44	1.65	1.74	1.79	1.83	1.86	1.89
	16	0.630	0.75	1.13	1.33	1.41	1.48	1.53	1.58	1.64
	19.05	0.75	0.59	0.97	1.17	1.25	1.32	1.36	1.41	1.46
	25.4	1	0.25	0.64	0.84	0.92	0.97	1.01	1.05	1.09
	32	1.260	-0.10	0.30	0.49	0.57	0.62	0.65	0.67	0.70

lightweight concrete, where the coarse aggregate is often weaker than the cement paste, allowing crack propagation through the aggregates. A recent study showed that the KCC model can provide excellent results if properly calibrated for these materials [20].

3. Strain-softening

In the presence of strain-softening, FE predictions will not provide objective solutions unless localization limiters are introduced. A number of methods have been proposed including direct length scale techniques (e.g., the "crack band" fracture model [21-22]), introduction of artificial viscosity or rate dependency [23], non-local methods [24-25], or microplane methods [26]. All of these methods have some limitations: the crack band assumes a localization width (which could be the element size), the rate dependency is limited to a rate range and loses effectiveness in the quasi-static limit, non-local methods rely on a zone of influence, and the microplane method is limited by the angle between microplanes. Some of the approaches (e.g. the last two) can be computationally intensive; hence a simple method was implemented in the model. The crack band method was implemented in two ways in Release III: the first is used for the generic concrete model and the second is intended for advanced use of the model where sufficient data is available from which to directly calibrate the model parameters.

For the generic concrete model, the crack band is assumed to occur within one element. The regularization is accomplished by internally scaling the softening branch of the damage function, $\eta(\lambda)$, using the average size of each element. Results illustrating the effectiveness of the approach are shown in Fig. 2. Here the results of single element simulations loaded in unconfined uniaxial tension (UUT) under velocity control are shown for four different element sizes. On the left of the figure, the stress versus strain response of the elements shows that for small elements, the softening is slow, while for larger elements, the softening is accelerated. On the right, the fracture energy, which is obtained by integrating the stress versus displacement response for each element, is plotted as a function of the displacement. Despite a small error, the fracture energies for each of the elements are very close to that in Table 1. Note that this regularization has limitations: it is not implemented when the element size exceeds 250 mm (the softening branch becomes vertical and the energy dissipated can no longer be reduced to match G_f), or when the elements are much smaller than the localization width (when the softening branch may approach a plastic limit, resulting possibly in excessive energy dissipation, e.g., in penetration problems).
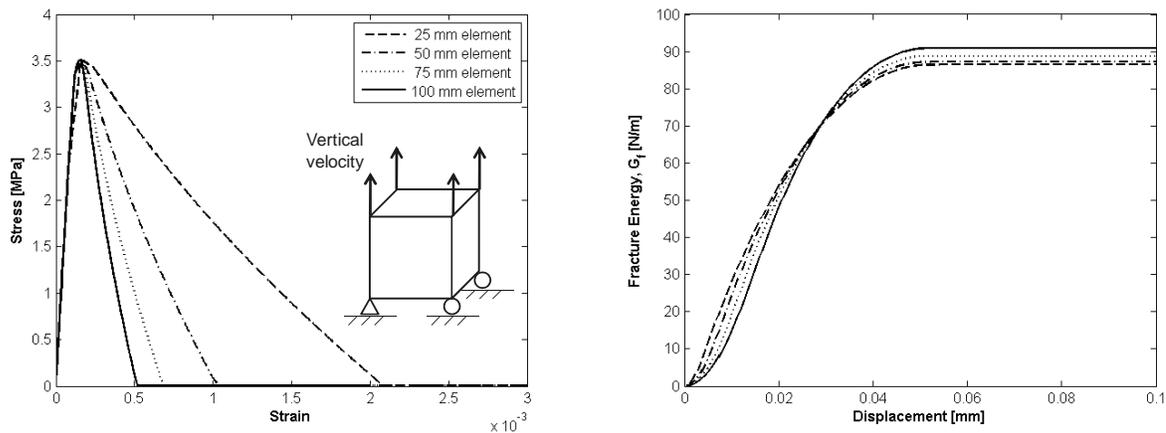
Fig. 2. Single element response in UUT using the generic concrete model (40 MPa, 16 mm MAS).

For user-defined material parameters, this regularization scheme may be insufficient if the parameters of $\eta(\lambda)$ are significantly different from the generic concrete material. The fracture energy regularization surface (FERS) approach was developed to provide means from which to preserve fracture energy in such cases. The FERS is a three-dimensional response surface, which the KCC model can use to compute a value for b_2 that considers the element size and the user-input G_f value. The FERS is defined as:

$$b_2 = \beta_0 + \beta_1 \cdot x_1 + \beta_2 \cdot x_2 + \beta_{12} \cdot x_1 \cdot x_2 + \beta_{11} \cdot x_1^2 + \beta_{22} \cdot x_2^2 + \beta_{111} \cdot x_1^3 + \beta_{222} \cdot x_2^3 \tag{4}$$

where, x_1 is the average element size (internally calculated for each element in LS-DYNA), x_2 is the desired G_f value, and β_i are the parameters of the FERS. In practice, one may execute numerous single-element or multi-element LS-DYNA simulations, using various mesh sizes and values for b_2, and the β_i parameters for Eqn (4) can be obtained using standard regression methods to obtain suitable FERS parameters.

An example is shown in Fig. 3, where the resulting fracture energies were computed for about one hundred UUT simulations using a single element, whose size and b_2 parameters were varied. The LS-DYNA results are shown as dots in the plot. The FERS surface is also shown in the figure, the parameters of which were obtained using nonlinear regression. The parameters of the FERS surface can then be input to the model, using a *DEFINE_LOAD_CURVE, which the KCC model uses to regularize the fracture energy for each element in the model.

A key benefit to this approach lies in the fact that the FERS need not be calibrated to single-element simulations, but can be based on the results for multi-element models under dynamic loads. In practice, this method may implicitly compensate for some of the limitations we discussed related to the localization width.
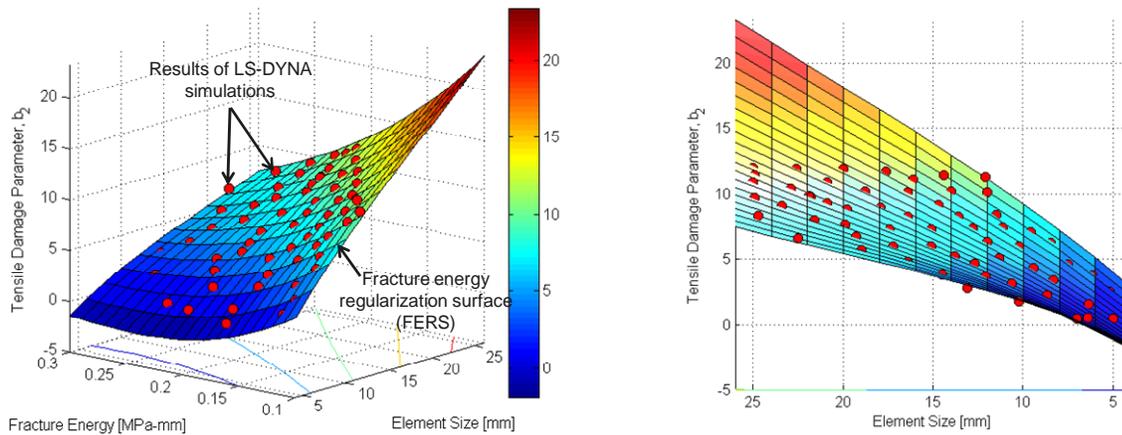
Fig. 3. Fracture energy regularization surface fit to single element simulations.

4. Rate effects

Loading rate effects in concrete have been recognized for decades [5, 27-28]. For typical structural response problems that were the focus of the concrete structures research community during this time, the DIF versus strain rate relationship for most constitutive models were calibrated directly to peak strength data like those obtained using the split-Hopkinson pressure bar (SHPB) [29]. Concrete data obtained from such tests exhibit a two branch behavior when plotted with normalized peak strength versus strain rate [5, 16, 27-28]. (Note that for brittle materials like unconfined concrete, strain rates in SHPB tests are rarely constant even though they are typically reported as such.)

Rate effects in concrete are due initially to moisture, and, at higher strain rates, to inertia effects [30]. Hence the initial branch of the DIF (e.g. below about 1.0 s^{-1}) should typically be included, as the constitutive model does not generally include the effects of moisture. The second branch of the DIF can be captured by the FE model, assuming adequate mesh resolution to do so. Consequently, there have been two schools of thought on this second branch, one advocating not using it to prevent duplication of inertia effects, and another one advocating its use to ensure proper dissipation. In practice, FE models are capable of capturing the inertia effects in compression (e.g. from the mass of the outer cylinder elements resisting motion laterally), but not as well in tension (since the model cannot capture the aggregate interlocking that propagates the microcracking and energy dissipation beyond the localization zone).

These concepts are illustrated in Fig. 4, where simulations of a well characterized concrete material were loaded in compression and tension. Two idealized loading variants are performed: (a) a quasi-static loading ($1.0e^{-4}$ s^{-1}) and (b) a dynamic loading pulse that induces global strain rates of approximately 100 s^{-1}. Three different mesh sizes are examined using the *rate-independent* version of the KCC model (i.e., by setting the DIF versus strain rate curve equal to unity). In compression, there is a clear increase in strength computed in the simulation when loaded dynamically as compared with the quasi-static case. This indicates that the FE model captures an inertia effect. For tension, no such increase is discernable, which indicates that a DIF function is needed to properly represent the inertia effect. Recently analytic and experimental studies have reinforced these notions [31-33].

Fig. 5 demonstrates that, in compression, only the initial branch of the DIF is needed to properly represent data from SHPB tests. Here, a 76.2 mm diameter SHPB compression test is simulated with a detailed FE model of the test (Fig. 5a) using KCC model parameters calibrated to quasi-static material characterization data for that material [13]. The actual loading pulses measured by the incident bar strain gauge are applied to the model for three different loading pulse levels designated "low", "medium", and "high" strain rates, and the results are compared with the output stress wave measured by the transmitter bar strain gauge. Three models are used to obtain numerical results for each of the three compression loading pulses: (1) Model 1, which uses the *rate-independent* model, (2) Model 2, which uses the modified CEB DIF with both branches of the function, and (3) Model 3, which uses the modified CEB DIF with only the first branch of the function (Fig. 5b). The resulting transmitted pulses are shown in Fig. 5c that can be compared with the experimental data. As expected, Model 1 produces peak strengths that are lower than the experiments (because that model does not account for the rate effects from moisture in the sample). Model 2 produces much higher peak strengths (in essence, double counting for inertia in the sample). Model 3, on the other hand, provides good agreement with the dataset, even though the DIF function (using only the first branch) was not calibrated to this specific concrete (i.e., the modified CEB model was used). These DIF factors (i.e., using both branches in tension and only the first one in compression) are representative of those needed as input to the model. It is possible, using this type of high-quality SHPB data for a particular concrete material, to improve DIF parameter estimates using parameter identification techniques.

5. Conclusions

This paper described recent improvements to Release III of the K&C concrete model, which was made available in LS-DYNA starting with v971. An automatic input capability is now provided as a tool for generating model parameters for generic concrete materials when little is known other than the concrete's compressive strength. There are, naturally, a number of limitations to this approach, which were reviewed and should be considered prior to deploying the generic model parameters. In addition, the model now includes improved methods from which to reduce mesh-dependencies due to strain-softening. Two methods are available: the first is used for the generic concrete model and the second is intended for advanced use of the model where sufficient data is available from which to directly calibrate the model parameters. The latter is attractive in that it provides a means from which to calibrate the parameters using the results of single or multi-element FE models. Lastly, concrete loading rate effects were discussed and guidance was provided on properly characterizing those effects with the KCC model. An example was shown that provides excellent results with test data.
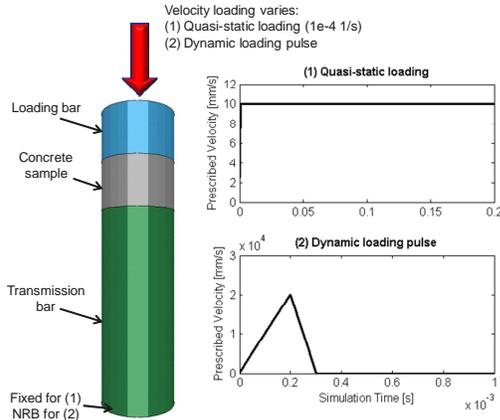
(a) Compression model.
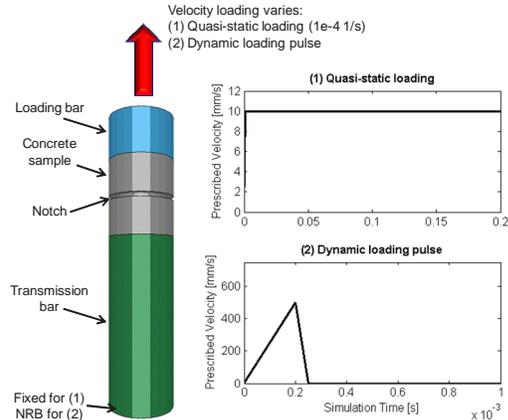
(b) Tension model.
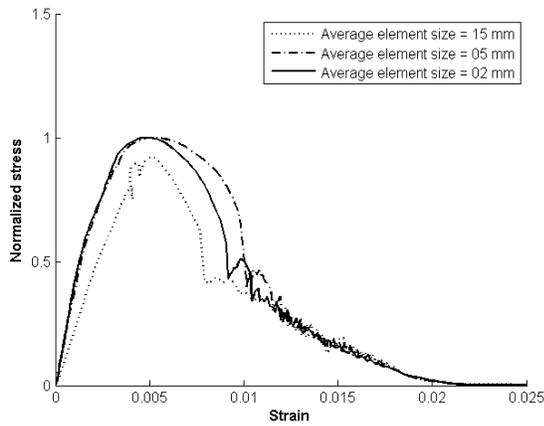
(c) Quasi-static compression loading.
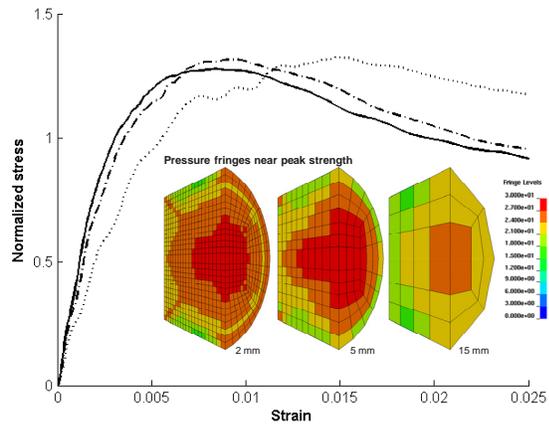
(d) Dynamic compression loading.
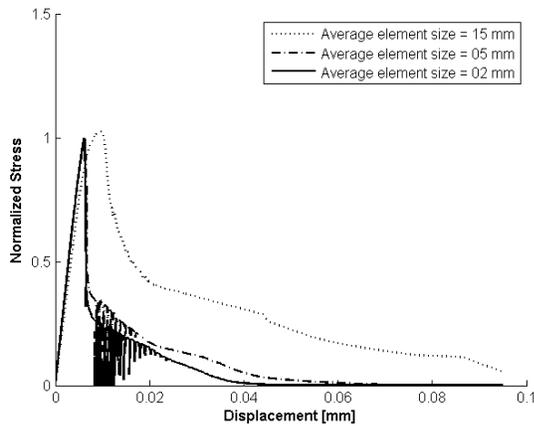
(e) Quasi-static tension loading.
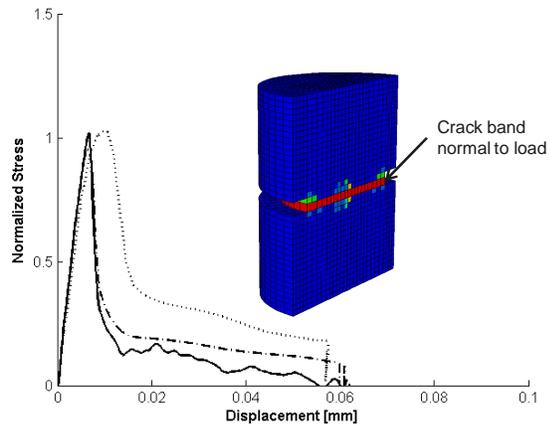
(f) Dynamic tension loading.

Fig. 4. Simulations of a concrete sample subjected to compression and tension; all results are computed using the *rate-independent* version of the KCC model.
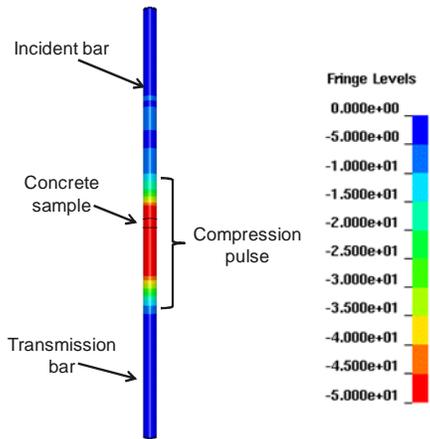
(a) Axial stress fringes in the SHPB.
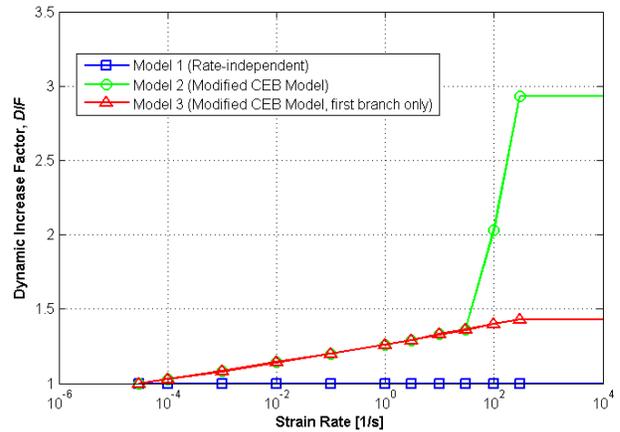
(b) Input DIF versus strain rate curves (compression).
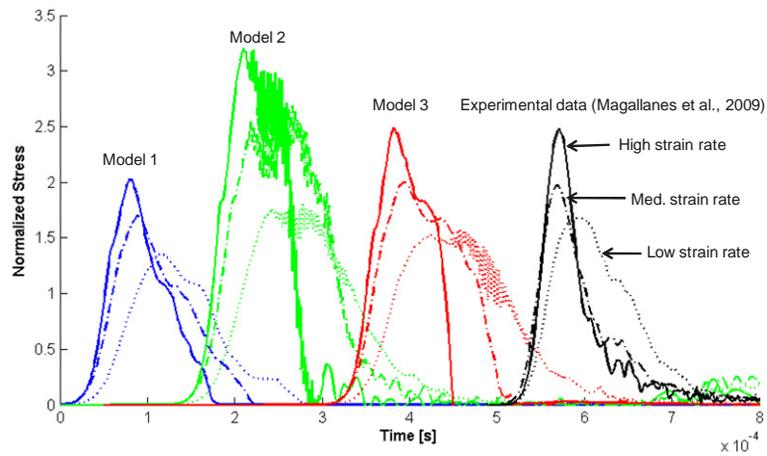
(c) Transmitted stress pulses as a function of time.
(Each of the groups of results is time shifted so that they may be examined individually).

Fig. 5. Comparisons of compression SHPB data with simulations using the KCC model.

6. Acknowledgements

7. References

[1] Malvar, L.J., Crawford, J.E., Wesevich, J.W., Simons, D. (1994), "A New Concrete Material Model for DYNA3D," TM-94-14.3, Report to the Defense Nuclear Agency, Karagozian and Case, Glendale, CA.

[2] Malvar, L.J., Crawford, J., Simons, D., Wesevich, J.W. (1995), "A New Concrete Material Model for DYNA3D," Proceedings, 10th ASCE Engineering Mechanics Conference, Vol. 1, Boulder, CO, pp. 142-146.

[3] Malvar, L.J., Crawford, J.E., Wesevich, J.W., Simons, D. (1997), "A Plasticity Concrete Material Model for DYNA3D," International Journal of Impact Engineering, Vol. 19, No. 9/10, pp. 847-873.

[4] Malvar, L.J., Crawford, J.E., Wesevich, J.W., Simons, D. (1996), "A New Concrete Material Model for DYNA3D - Release II: Shear Dilation and Directional Rate Enhancements," TR-96-2.2, Report to the Defense Nuclear Agency, Karagozian and Case Structural Engineers, Glendale, CA. *(Limited Distribution)*

[5] Malvar, L.J., Crawford, J.E. (1998), "Dynamic Increase Factors for Concrete," Proceedings of the 28th DDESB Explosive Safety Seminar, Orlando, FL, August.

[6] Livermore Software Technology Corporation (2007a), "LS-DYNA Keyword User's Manual: Volume I," Version 971, Livermore, CA.

[7] Livermore Software Technology Corporation (2007b), "LS-DYNA Keyword User's Manual: Volume II, Material Models," Version 971, Livermore, CA.

[8] Crawford, J.E., Malvar, L.J. (1997), "User's and Theoretical Manual for K&C Concrete Model," TR-97-53.1, Karagozian and Case Structural Engineers, Glendale, CA. *(Limited Distribution)*

[9] Magallanes, J.M. (2008), "Importance of concrete material characterization and modeling to predicting the response of structures to shock and impact loading," Structures Under Shock and Impact X, Eds. N. Jones, WIT Press, Southampton.

[10] Malvar, L.J., Morrill, K.B., Crawford, J.E. (2004), "Numerical Modeling of Concrete Confined by Fiber Reinforced Composites," Journal of Composites for Construction, Vol. 8, No.4, pp. 315-322.

[11] Bao, X., Li, B. (2010), "Residual Strength of Blast Damaged Reinforced Concrete Columns," International Journal of Impact Engineering, Vol. 37, No. 3, pp. 295-308.

[12] Tu, Z., Y. Lu, Y. (2009), "Evaluation of typical concrete material models used in hydrocodes for high dynamic response simulations," International Journal of Impact Engineering, Vol. 36, No. 1, pp. 132-146.

[13] Magallanes, J.M., Martinez, R.M., Neser, A., Schreiber, D., Zencker, U. (2009), "A Comprehensive Material Testing Program for Characterizing Concrete Behaviors Under Static and Dynamic Loads," Proceedings of the 13th International Symposium on the Interaction of the Effects of Munitions with Structures (ISIEMS), Brühl, Germany.

[14] Chen, W.F. (1982), Plasticity in Reinforced Concrete, McGraw Hill, New York.

[15] Malvar, L.J., Crawford J.E., Morrill, K.B. (1999), "K&C Concrete Material Model, Release III: Automated Generation of Material Model Input," TR-99-24, Karagozian and Case Structural Engineers, Glendale, CA. *(Limited Distribution)*

[16] Comité Euro-International du Béton - Fédération Internationale de la Précontrainte (1990), CEB-FIP Model Code 90, Redwood Books, Trowbridge, Wiltshire, Great Britain (ISBN 0-7277-1696-4).

[17] Imran, I., Pantazopoulou, S.J. (1996), "Experimental Study of Plane Concrete under Triaxial Stress," ACI Materials Journal, Vol. 93, No. 6, pp. 589-601.

[18] Gabet, T., Malecot, Y., Daudeville, L. (2008), "Triaxial behavior of concrete under high stresses: Influence of the loading path on compaction and limit states," Cement and Concrete Research, Vol. 38, pp. 403-412.

[19] Vu, X. H., Malecot, Y., Daudeville, L., Buzaud, E. (2009), "Experimental analysis of concrete behavior under high confinement: Effect of the saturation ratio," International Journal of Solids and Structures, Vol. 46, pp. 1105-1120.

[20] Magallanes, J.M., Morrill, K.B., Crawford, J.E. (2008), "Finite element models for the analysis and design of CMU walls to blast loads," Proceedings of the 80th DDESB Explosives Safety Seminar, Palm Springs, CA.

[21] Bažant, Z.P., Oh, B.H. (1983), "Crack bank theory for fracture of concrete," Materials and Structures, Vol. 16, pp. 155-177.

[22] Oliver, J. (1989), "A Consistent Characteristic Length for Smeared Cracking Models," International Journal for Numerical Methods in Engineering," Vol. 28, pp. 461-474.

[23] Sandler, I., Wright, J. (1984), "Summary of strain-softening," In Theoretical Foundations for Large-Scale Computations of Nonlinear Material Behavior, DARPA-NSF Workshop, Edited by N. Nemat-Nasser, pp.285-315, Northwestern University.

[24] Pijaudier-Cabot, G., Bažant, Z.P. (1987), "Nonlocal Damage Theory," Journal of Engineering Mechanics, Vol. 113, No. 10, pp. 1512-1533.

[25] Belytschko, T., Bažant, Z.P., Hyun, Y.W., Chang, T.P. (1986), "Strain-Softening Materials and Finite-Element Solutions," Computers and Structures, Vol. 23, No. 2, pp.163-180.

[26] Bazant, Z.P., Prat, P.C. (1988), "Microplane Model for Brittle-Plastic Materials, I. Theory and II. Verification," Journal of Engineering Mechanics, Vol. 114, No. 10, pp. 1672-1702.

[27] Ross, C.A., Thompson, P.Y., Tedesco, J.W. (1989), "Split-Hopkinson Pressure-Bar Tests on Concrete and Mortar in Tension and Compression," ACI Material Journal, Vol. 86, No. 5, 9pp. 475-481.

[28] Ross, C.A., Jerome, D.M., Tedesco, J.W., Hughes, M.L. (1996), "Moisture and Strain Rate Effects on Concrete Strength," ACI Materials Journal, Vol. 93, No. 3, pp. 293-300.

[29] Gray, G.T. (1999), "Classic Split-Hopkinson Pressure Bar Technique: Chapter 6A," Los Alamos National Laboratory Technical Report, LA-UR-99-2347.

[30] Malvar, L.J., Ross, C.A. (1999), Closure to the Discussion of "Review of Static and Dynamic Properties of Concrete in Tension," by Toutlemonde F. and Rossi P., ACI Materials Journal, Vol. 96, No. 5, pp. 614-616.

[31] Cotsovos, D.M., Pavlović, M.N. (2008), "Numerical investigation of concrete subjected to compressive impact loading. Part 1: A fundamental explanation for the apparent strength gain at high loading rates," Computers and Structures, Vol. 86, No. 5, pp. 145-163.

[32] Zhang, M., Wu, H.J., Li, Q.M., Huang, F.L. (2009), "Further investigation on the dynamic compressive strength enhancement of concrete-like materials based on split Hopkinson pressure bar tests. Part I: Experiments," International Journal of Impact Engineering, Vol. 36, No. 12, pp. 1327-1334.

[33] Kim, D.J., Sirijaroonchai, K., El-Tawil, S., Naaman, A.E. (2010), "Numerical simulation of the Split Hopkinson Pressure Bar test technique for concrete under compression," International Journal of Impact Engineering, Vol. 37, No. 2, pp. 141-149.